Angular distributions of high-order harmonics generated by a femtosecond laser

Salieres, P; Ditmire, T; Perry, M. D; L'Huillier, Anne; Lewenstein, M

Published in:
Journal of Physics B: Atomic, Molecular and Optical Physics

DOI:
10.1088/0953-4075/29/20/027

1996

Angular distributions of high-order harmonics generated by a femtosecond laser

1996 J. Phys. B: At. Mol. Opt. Phys. 29 4771

(http://iopscience.iop.org/0953-4075/29/20/027)

J. Phys. B: At. Mol. Opt. Phys. **29** (1996) 4771–4786. Printed in the UK

Angular distributions of high-order harmonics generated by a femtosecond laser

P Salières†, T Ditmire‡‖, M D Perry‡, A L'Huillier†§ and M Lewenstein†

† Commissariat à l'Energie Atomique, DSM/DRECAM/SPAM, Centre d'Etudes de Saclay, 91191 Gif-sur-Yvette, France

‡ Laser Program, Lawrence Livermore National Laboratory, PO Box 808, L-439 Livermore, CA 94551-9000, USA

§ Department of Physics, Lund Institute of Technology, S-221 00 Lund, Sweden

Received 15 April 1996, in final form 9 July 1996

Abstract. We present a systematic study of the angular distributions of high-order harmonics generated with a femtosecond Cr:$LiSrAlF_6$ laser. We investigate the influence of different parameters, namely laser intensity, nonlinear order, nature of the gas and position of the laser focus relative to the generating medium. We show that when the laser is focused before the atomic medium, harmonics with regular spatial profiles can be generated with reasonable conversion efficiency. Their divergence does not depend *directly* on the nonlinear order, the intensity or even the nature of the generating gas, but rather on the *region of the spectrum* the considered harmonic belongs to, which is determined by the combination of the three preceding elements. When the focus is drawn closer to the medium, the distributions get increasingly distorted, becoming annular with a significant divergence for a focus right into—or after—the jet. We perform numerical simulations of the angular distributions. The simulated profiles reproduce remarkably well the experimental trends and are thus used to interpret them.

1. Introduction

Over the past few years, high-order harmonic generation has become one of the most promising ways of producing short-pulse coherent radiation in the XUV range. By focusing short-pulse terawatt lasers in rare gas jets, wavelengths as short as 7.4 nm (109th harmonic of an 806 nm Ti-Sapphire laser (Macklin *et al* 1993)) and, more recently, 6.7 nm (37th harmonic of a 248 nm KrF laser (Preston *et al* 1996)) have been obtained. The spatial characterization of such radiation provides useful information from a double standpoint. It gives information on the spatial coherence of the beam and on its focusability, which are of interest for applications. Moreover, it helps in understanding the physics of the process, providing more detailed information than the usual measurement of the total integrated harmonic signal. There are many possible causes for distortion of the spatial profiles, and their interpretation implies a rather refined study, demanding deep understanding.

The harmonic spatial profiles reported so far have been obtained in different experimental conditions. Peatross and Meyerhofer (1995) used a 1 μm 1 ps Nd-Glass laser loosely focused (f/70) into a very diluted gaseous media (1 Torr) in order to get rid of distortions induced by phase matching and propagation in the medium. Since volume effects become negligible, the generated harmonic field can then be considered as coming from a plane at the laser

‖ Present address: Blackett Laboratory, Imperial College, Prince Consort Road, London SW7 2BZ, UK.

0953-4075/96/204771+16$19.50

focus, and is characteristic of the single-atom response. The far-field distributions of the harmonics (11 to 41) generated in heavy rare gases are found to be quite distorted, with broad wings surrounding a narrow central peak. These wings are attributed to the rapid variation of the harmonic dipole phase with the laser intensity.

Tisch *et al* (1994) studied high-order harmonics (71 to 111) generated by a similar laser, focused (f/50) in 10 Torr of helium. Complex spatial distributions are found for harmonics in the plateau region of the spectrum. However, in the cut-off, the measured angular distributions narrow to approximately that predicted by lowest-order perturbation theory. The broad distributions with numerous substructures observed in the plateau are attributed to the influence of ionization, and in particular of the free electrons, on phase matching. Muffet *et al* (1994) modelled these results, and showed that, depending on the focusing conditions, substructures could be either due to ionization or to resonances in the intensity dependence of the atomic phase.

The influence of ionization on spatial profiles has also been investigated experimentally by L'Huillier and Balcou (1993) for low-order harmonics in xenon, and, more recently, by Wahlström *et al* (1995) for harmonics generated by rare-gas-like ions. Generally speaking, ionization induces a significant distortion of the harmonic profiles, thus complicating their interpretation.

In a recent letter (Salières *et al* 1994), we presented results of an experimental study of spatial profiles of harmonics generated by a 140 fs $Cr:LiSrAlF_6$ (Cr:LiSAF) laser system. Thanks to this very short pulse duration, it was possible to expose the medium to high intensities while keeping a weak degree of ionization. Under certain conditions, the resulting harmonic profiles were found to be very smooth, Gaussian to near flat-top, without substructure. This behaviour was discussed in a theoretical paper by Salières *et al* (1995) and interpreted in terms of the intensity dependence of the harmonic dipole phase in the tunnelling regime. When the considered harmonic is in the cut-off region of the spectrum, where the harmonic strength increases steeply with intensity, the dipole phase decreases slowly and linearly. In the plateau region, the dipole strength saturates whereas the phase decreases twice as fast as before with superimposed oscillations. This quick intensity dependence of the dipole phase has a strong influence on the way the generated harmonic field and the nonlinear polarization are phase matched. In particular, it induces a dramatic dependence of the spatial profiles on the focusing geometry, and especially on the laser focus position relative to the gas jet.

In the present paper, we give a full account of our experimental studies concerning angular profiles in different conditions. Systematic measurements of the harmonic spatial profiles were performed in argon and neon as a function of nonlinear order, laser intensity, and position of the laser focus relative to the jet. The wide range investigated for these parameters allows us to generalize to different orders and intensities. This paper is organized as follows. In section 2, we describe the laser system and the experimental apparatus and method. The influence of the position of the laser focus relative to the jet is investigated in section 3. The dependences of the profiles on laser intensity and nonlinear order are studied, respectively, in sections 4 and 5. Finally, we present in section 6 numerical simulations of the spatial profiles which help us to give an interpretation of the results. We summarize in section 7.

2. Description of the experiment

The laser system used was the Cr:LiSAF-based laser developed at the Lawrence Livermore National Laboratory and described in detail in Ditmire *et al* (1994). The main advantage

of the Cr:LiSAF material, besides a broad gain band comparable to Ti:Sapphire, is its long upper-state lifetime which allows for direct flashlamp pumping, leading to compact terawatt systems. The system begins with a self-mode-locked Ti:Sapphire oscillator which produces 110 fs pulses of 8 nJ at 76 MHz. The pulse train is first injected into a diffraction grating stretcher, which widens the pulses to 500 ps, and then into a regenerative amplifier ring cavity, utilizing a 4 mm flashlamp-pumped 2% doped Cr:LiSAF rod as amplifying medium. After 34 round trips achieving a total net gain of 5×10^6, a single pulse is switched out by a Pockels cell. It is then amplified in a 4 mm and two 9.5 mm Cr:LiSAF amplifiers. After spatial filtering in vacuum, the pulse is recompressed in a grating pair compressor to a near-transform limited 135 fs width. This system can produce 280 mJ pulses at 825 nm with a 1 Hz repetition rate, which allows for systematic studies. The spatial characteristics of this laser have been optimized by relay imaging and spatial filtering techniques. The profile is near-flat-top (super-Gaussian), with a total diameter of 4.2 cm. In our experiment, it was focused by an 85 cm focal length lens to a mean diameter of 150 μm, the spot being slightly elliptical with a 0.8 roundness (ratio of the minor to the major axes of the intensity ellipse). The divergence after the focus was measured to be 55 mrad (full width at $1/e^2$). This corresponds to about three times the diffraction limit.

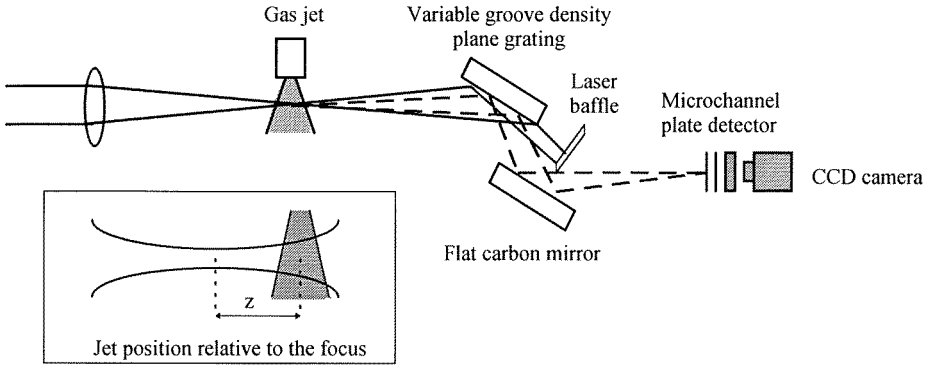

Figure 1. Experimental set-up for harmonic generation and measurement of the angular distributions. The position of the gas jet relative to the laser focus is called z as shown in the inset.

A schematic of the experimental set-up is shown in figure 1. The nonlinear medium was provided by a General-Valve pulsed gas jet which produces pressures between 10 and 100 Torr depending upon backing pressure. The density has not been measured precisely in this experiment, but we checked that the spatial profiles were independent of the backing pressure over a large range (300 to 1000 Torr). In our experimental conditions, the number of clusters present in the jet was negligible. The position of the gas jet relative to the laser focus is called z (see the inset in figure 1). z is taken positive for a focusing before the gas jet. Though not measured accurately in this experiment, the z position referred to in section 3 was inferred from comparison with the numerical simulations presented in section 6.

The harmonics produced were spectrally dispersed by a flat-field spectrometer consisting of a variable groove density (approximately 1200 grooves mm^{-1}) plane grating and a flat carbon mirror. In order to optimize the collection efficiency, no entrance slit was used. A baffle, placed above the carbon mirror, intercepted the laser beam reflected by the grating. The harmonics were detected in the focal plane by a system of CsI-coated dual microchannel

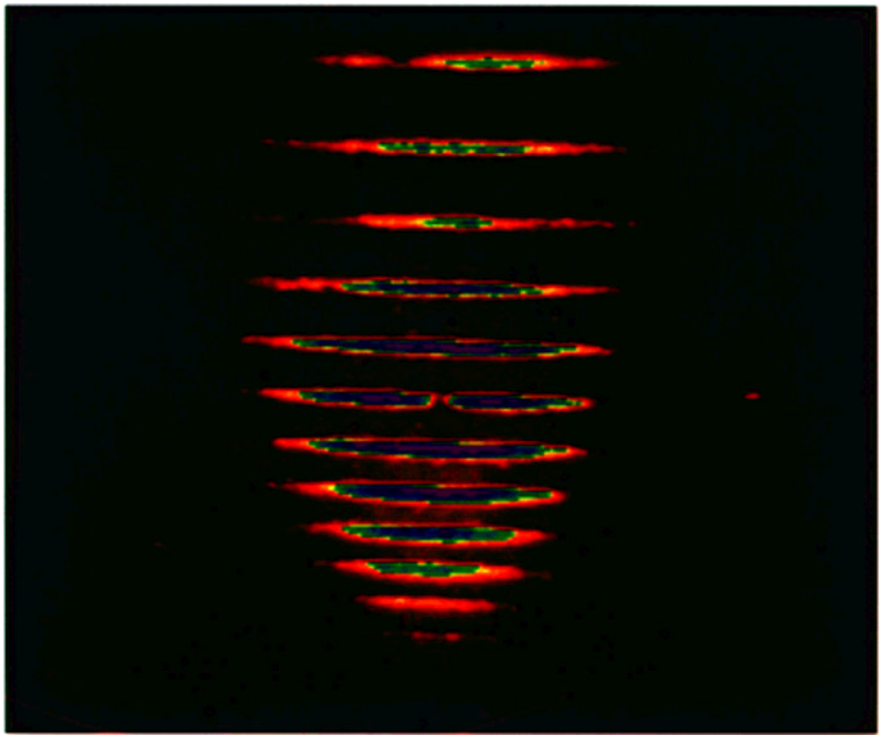

Figure 2. Image obtained in neon at 2.7×10^{14} W cm^{-2} and $z = 3$ mm. The vertical direction is the spectrum going towards shorter wavelengths from the top to the bottom. The horizontal direction is the spatial profile. Harmonics from the 25th to the 47th are displayed.

plates (MCP) coupled to a phosphorus screen (Galileo VUV-25), which was read by an 8-bit CCD camera (IMC-500).

The data acquisition consisted in taking the average of five images recorded by the CCD camera, selected with an energy window of $\pm 10\%$. The images were extremely reproducible on a shot-to-shot basis, and the averaging procedure was used essentially to minimize the noise level. A typical image is shown in figure 2. The vertical axis is the spectral dispersion going to shorter wavelengths from the top to the bottom. The spatial profile of the harmonics is shown horizontally, with the intensity represented by the different colours. By integrating these profiles, we can study the total harmonic signal as a function of the harmonic order. Over the spectral range displayed by the MCP, the responses of the spectrometer and of the MCP are essentially flat and we can therefore determine which harmonics are in the plateau or in the cut-off at the considered intensity. Figure 2 displays the 25th to the 47th harmonic generated in neon at a peak intensity (at focus) of 2.7×10^{14} W cm^{-2} and a focus position 3 mm before the gas jet. Note that dead channels of the MCP located on the side of the 25th and 29th and at the centre of the 35th harmonic lead to a distortion of the corresponding profiles. Beyond the 37th order, harmonics are less and less intense and therefore correspond to the cut-off region of the spectrum. From the analysis of images taken at different intensities, we can determine the plateau–cut-off transition intensities corresponding to different harmonic orders. Some of them are listed in table 1 (for neon as nonlinear medium and $z = 3$ mm) together with the saturation intensity for ionization of neon measured by Wahlström *et al* (1993) in similar conditions. In argon spectra, the

Table 1. Plateau–cut-off transition intensities corresponding to different harmonic orders generated in neon in $z = 3$ mm. The saturation intensity for ionization of neon is also indicated.

Harmonic order	Plateau–cut-off transition intensity
H37	2.7×10^{14} W cm^{-2}
H45	5.1×10^{14} W cm^{-2}
H51	7.0×10^{14} W cm^{-2}
Isat (from Wahlström *et al* (1993))	8.0×10^{14} W cm^{-2}

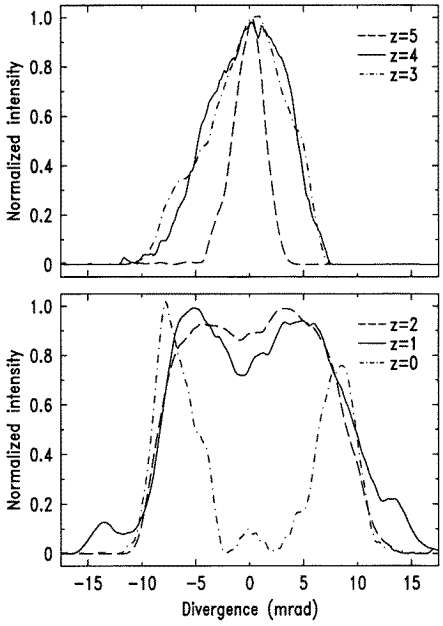

Figure 3. Spatial profiles of the 39th harmonic generated in neon at a peak intensity of 3×10^{14} W cm^{-2} for different locations z of the medium relative to the laser focus, indicated in mm in the figure.

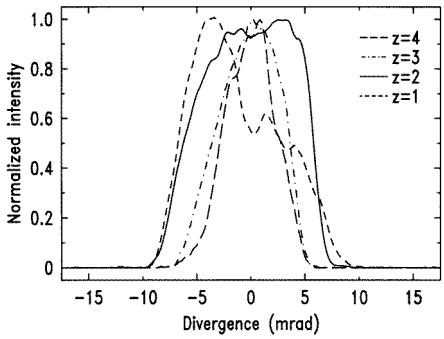

Figure 4. Spatial profiles of the 45th harmonic generated in neon at a peak intensity of 3×10^{14} W cm^{-2} for different locations z of the medium relative to the laser focus, indicated in mm in the figure.

plateau–cut-off transition is less clear than in neon due to the low saturation intensity for ionization (2.5×10^{14} W cm^{-2} from the above reference).

We now present horizontal lineouts of selected images in order to study the influence of different parameters. We begin with the study of the influence of the position of the gas jet relative to the laser focus on the spatial profiles, which is the most critical parameter.

3. Experimental study of the influence of the relative jet/focus position

We present in figures 3–4 a series of measurements in neon performed at different positions z of the jet relative to the laser focus. Images were recorded when moving the jet lengthwise with a 1 mm step, keeping a constant laser energy. The laser energy was chosen so that the intensity at best focus is around 3×10^{14} W cm^{-2}, and hence much smaller than the saturation intensity for ionization in neon (8×10^{14} W cm^{-2}) in order to avoid possibly additional distortion due to ionization. The MCP bias voltage, and consequently the detector

gain, was adjusted at each position in order to maintain approximately the same signal level.

We show in figure 3 the spatial profile of the 39th harmonic for several jet positions, covering a 5 mm range. For clarity we represent the profiles in two graphs. The evolution is very clear: when the atomic medium is placed much after the focus ($z = 5$ mm), the harmonic profile is very narrow with a maximum at the centre (6 mrad full divergence in $1/e^2$). When moving the jet towards the focus, the profile first broadens to 15 mrad ($z = 3$ mm), then flattens, becoming super-Gaussian ($z = 2$ mm). Then a dip appears at the centre of the profile ($z = 1$ mm). When the laser is moved into the jet ($z = 0$), the profile becomes completely annular with a total divergence of more than 20 mrad. For negative z, the profiles get even more annular while the conversion efficiency drops.

The result for the 45th harmonic obtained at the same laser intensity is presented in figure 4. This harmonic is close to the cut-off region of the spectrum and its spatial profile can be recorded only over 3 mm due to the low signal. The profiles are very similar to those of the 39th harmonic obtained at the same positions, but with smaller divergences. The distribution evolves from a narrow Gaussian (10 mrad at $z = 3$ mm) to a near flat-top profile ($z = 2$ mm) and eventually to an annular structure (16 mrad at $z = 1$ mm) which is not symmetric and does not appear clearly here due to a low resolution caused by the low signal.

In conclusion, there is a dramatic change of the shape as well as of the divergence of the harmonic spatial profiles with the position of the jet relative to the focus. This evolution occurs over a few millimetres, which is of the order of magnitude of the confocal parameter of the laser. On this scale, we would have expected little variation since the intensity distribution does not change much. Looking more carefully at the laser spot revealed that the beam presented a certain degree of astigmatism, but developed over a much longer distance. The small distortion of the laser spot cannot explain the dramatic change of the harmonic profiles.

The other important conclusion is that there are jet positions where regular spatial profiles can be generated with reasonable conversion efficiency. Quite surprisingly, these positions seem to be located significantly *after* the laser focus.

4. Experimental study of the influence of the laser intensity

We now present measurements of the spatial profiles as a function of the laser intensity at a given z position, chosen here to be $z = 3$ mm, where the spatial profiles are quite regular. Increasing the intensity, we can follow the evolution of the profile of a given harmonic when it leaves the cut-off region to enter the plateau.

Figure 5 shows the spatial profiles of the 45th harmonic generated in neon at different laser intensities, indicated in units of 10^{14} W cm^{-2} in the captions. At low intensity, when the harmonic is in the cut-off region, the profile is almost Gaussian with a very small divergence: 7 mrad at $1/e^2$ at 2.7×10^{14} W cm^{-2}. When the intensity is increased, the distribution broadens, becoming super-Gaussian, until its divergence reaches 12 mrad at 5.1×10^{14} W cm^{-2}. Beyond this intensity, corresponding to the transition to the plateau region, the shape of the profile does not change much, while the divergence increases slightly (14 mrad at 1.1×10^{15} W cm^{-2}). The latter is thus multiplied by a factor of 1.2 for a doubling of the intensity in the plateau region, instead of a factor of 1.7 in the cut-off region.

The spatial profiles for the 51st harmonic are shown in figure 6. Note that the small bump on the right-hand side of the profiles is simply due to a crack on the MCP. The evolution is very similar to that of the 45th harmonic, with the same shapes and divergences, but for

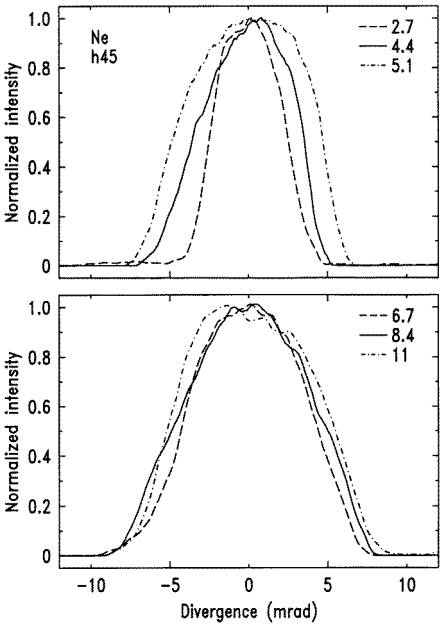

Figure 5. Spatial profiles of the 45th harmonic generated in neon at $z = 3$ mm for different laser intensities indicated in units of 10^{14} W cm^{-2} in the figure.

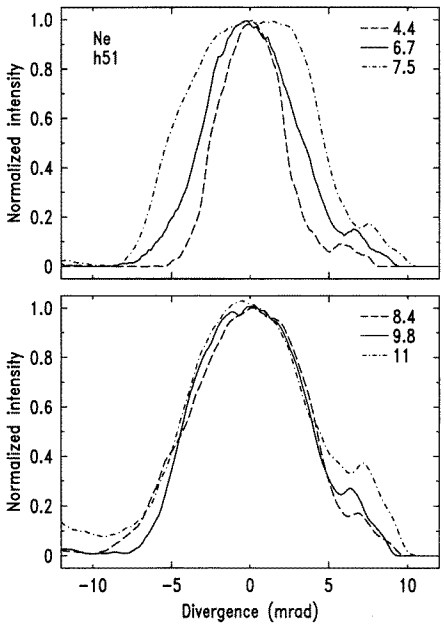

Figure 6. Spatial profiles of the 51st harmonic generated in neon at $z = 3$ mm for different laser intensities indicated in units of 10^{14} W cm^{-2} in the figure.

higher intensities. For example, the 7 mrad profile is obtained at 4.4×10^{14} W cm^{-2} instead of 2.7×10^{14} W cm^{-2} for the 45th harmonic, and the increase of the divergence saturates for intensities larger than 7.5×10^{14} W cm^{-2}.

This can simply be understood by noticing that the intensity of the plateau–cut-off transition of the 51st harmonic is larger than that of the 45th. Therefore, when the 45th harmonic reaches the plateau, where the divergence is large, the 51st is still in the cut-off region, with a narrow profile. This order dependence will be presented in more detail in the next section.

The spatial profiles for the 23rd harmonic generated in argon are shown in figure 7. At an intensity of $\times 10^{14}$ W cm^{-2}, this harmonic is in the cut-off region and exhibits a Gaussian profile similar to that of cut-off harmonics generated in neon, with the same divergence: 7 mrad. Increasing the intensity, the profile broadens to become triangular with a divergence of 14 mrad at 2×10^{14} W cm^{-2}. Beyond this intensity, it becomes increasingly distorted and flattened, finally to exhibit a ring around the central peak at 4.3×10^{14} W cm^{-2}. The latter distortions can be attributed to the effect of ionization on harmonic generation since they appear above the saturation intensity for ionization of argon (about 2.5×10^{14} W cm^{-2}, as measured by Wahlström *et al* (1993) in similar conditions).

Figure 8 presents the profiles of the 29th harmonic generated in argon. At low intensity, when the harmonic is far in the cut-off region, profile and divergence seem to be constant (1.5 and 1.8×10^{14} W cm^{-2}). Then the distribution broadens in a similar way to that of the 23rd harmonic, but for higher intensities.

As a conclusion, the results in argon and neon are very similar despite the different nonlinear orders considered. Profiles taken in the cut-off region all exhibit the same

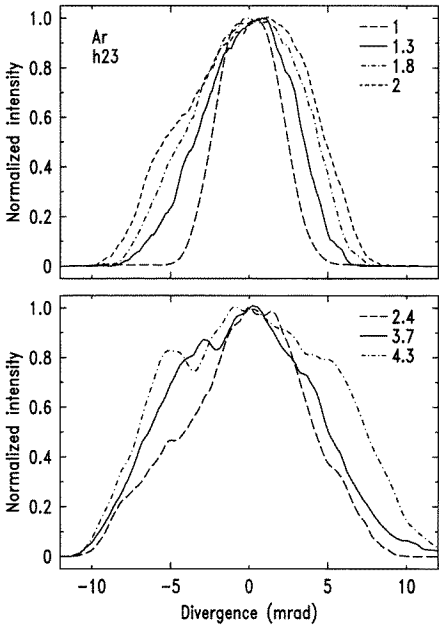

Figure 7. Spatial profiles of the 23rd harmonic generated in argon at $z = 3$ mm for different laser intensities indicated in units of 10^{14} W cm^{-2} in the figure.

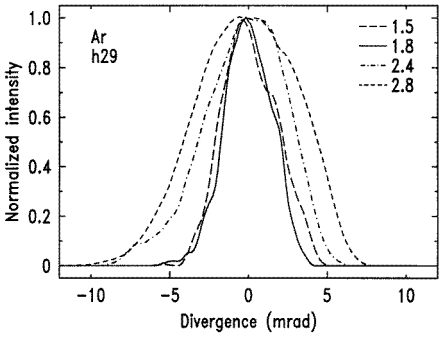

Figure 8. Spatial profiles of the 29th harmonic generated in argon at $z = 3$ mm for different laser intensities indicated in units of 10^{14} W cm^{-2} in the figure.

divergence (7 mrad) that increases with intensity to about 13 mrad. In argon, the divergence keeps increasing while the profile is distorted by ionization. In neon, the distributions stay approximately constant with a slight increase of the divergence. Note that the intensities used were not high enough to induce a significant degree of ionization in that case (the saturation intensity for ionization of neon is about 8×10^{14} W cm^{-2}).

5. Experimental study of the influence of the nonlinear order

We now compare spatial profiles for several harmonics at a given intensity, keeping the same z position ($z = 3$ mm) as before.

Figure 9 shows normalized profiles of harmonics generated in neon at 2.7×10^{14} W cm^{-2}, corresponding to the image shown in figure 2. We present in the first graph the 27th, 31st and 37th harmonics to illustrate the similarity of the super-Gaussian profiles of harmonics situated in the plateau region. Their divergence is about constant at 14 mrad. Beyond the 37th harmonic, which is at the end of the plateau, the distributions get narrower and narrower as the order increases: the divergence decreases quickly and regularly down to 7 mrad for the 45th harmonic, which is the last visible in the cut-off.

When the intensity is increased to 5.1×10^{14} W cm^{-2}, the 41st to 45th harmonics are no longer in the cut-off exhibiting narrow profiles, but rather in the plateau with large distributions, as can be seen in figure 10. The cut-off region is shifted to harmonics 47–53, with the same narrowing of the profiles as observed previously at the intensity 2.7×10^{14} W cm^{-2}.

The same effect can be observed in argon; the results obtained at 1.8×10^{14} W cm^{-2} are

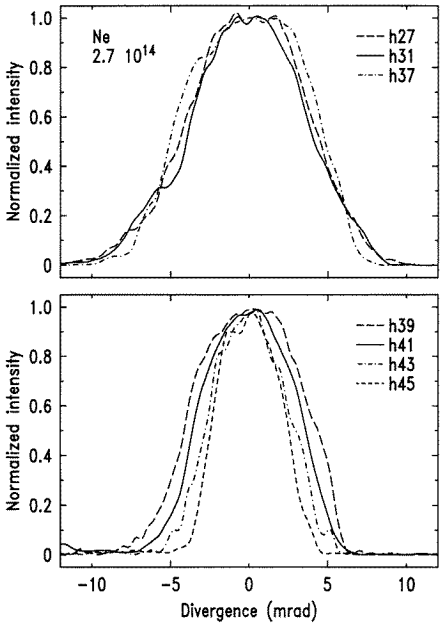

Figure 9. Spatial profiles of several harmonics located between the 27th and the 45th, generated in neon at $z = 3$ mm and at an intensity of 2.7×10^{14} W cm^{-2}.

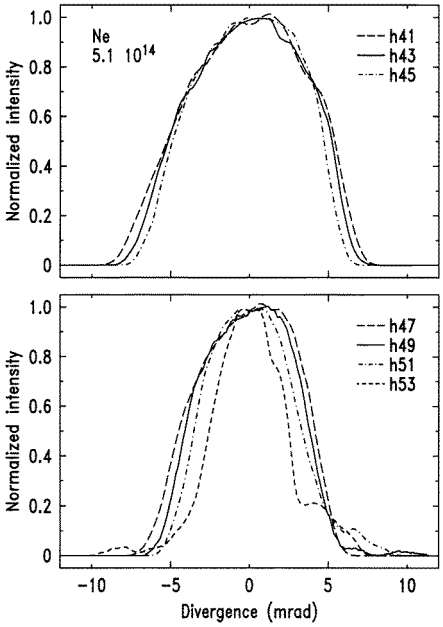

Figure 10. Spatial profiles of harmonics located between the 41st and the 53rd, generated in neon at $z = 3$ mm and at an intensity of 5.1×10^{14} W cm^{-2}.

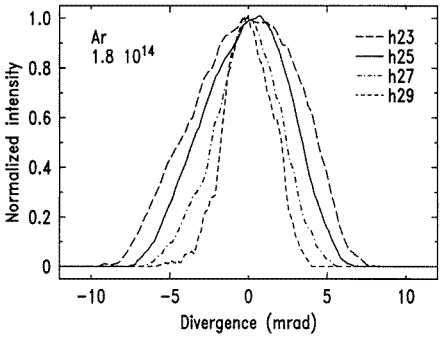

Figure 11. Spatial profiles of harmonics located between the 23rd and the 29th, generated in argon at $z = 3$ mm and at an intensity of 1.8×10^{14} W cm^{-2}.

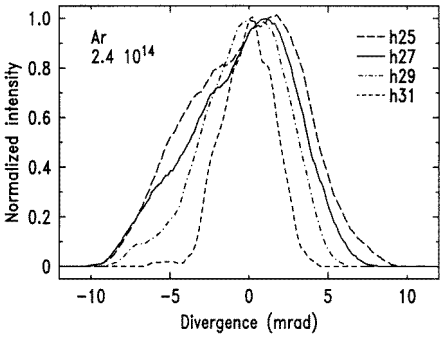

Figure 12. Spatial profiles of harmonics located between the 25th and the 31st, generated in argon at $z = 3$ mm and at an intensity of 2.4×10^{14} W cm^{-2}.

presented in figure 11. The 23rd harmonic, located at the end of the plateau region, exhibits a quasi-triangular profile with a 13 mrad divergence. For the harmonics in the cut-off, the divergence decreases quickly to reach 6 mrad for the 29th. The same evolution is obtained at 2.4×10^{14} W cm^{-2} but with a shift of one harmonic: figure 12 represents the profiles of harmonics 25 to 31, that are a little more distorted than previously.

We thus reach the same conclusion as in the preceding section, which we can now generalize to all (sufficiently high) harmonics generated in neon or in argon. The profile of a given harmonic does not depend *directly* on the nonlinear order, the intensity or even the nature of the generating gas, but rather on the *region of the spectrum* the harmonic belongs

to, which is determined by the combination of the three preceding elements.

The decrease of the divergence in the cut-off region has also been observed by Tisch *et al* (1993) for harmonics 71 to 111 of a glass laser in neon. However, the profiles of harmonics located in the plateau were distorted with many substructures. The much smaller ionization rate due to the smaller pulse duration of our laser (140 fs instead of 1 ps) may be an explanation for the lack of structures and the regularity of the profiles observed in our experiment. Indeed, we have seen in argon that high intensities were needed to distort the profiles. Another possible explanation could be the focusing geometry, and in particular the position of the focus relative to the generating medium. As shown in section 3, this relative position has a dramatic influence on the profiles and can be a cause of distortion. The difference between our results and those of Tisch *et al* would then be a consequence of a different location of the atomic medium relative to the gas jet.

6. Simulation and interpretation of the experimental dependences

6.1. Method

The interpretation of the experimental results presented above is not straightforward and requires good understanding of the physics involved in harmonic generation. In order to gain some insight into these processes, we have performed extensive numerical simulations in the experimental conditions.

The theoretical description of high-order harmonic generation requires the calculation of the single-atom response to the strong laser field, and the propagation of the generated harmonic fields in the medium. To deal with the first step, i.e. to calculate in a simple way the induced dipole moments in this low-frequency high-intensity regime, we used the model of Lewenstein *et al* (1994), which is a quantum formulation of the semiclassical model developed by Kulander *et al* (1993) and Corkum (1993). It allows us to calculate the amplitude and the phase of the harmonic components of the atomic dipole moment. These data are then inserted as source terms in the propagation equations for the harmonic fields, that are solved in the slowly varying envelope approximation (L'Huillier *et al* 1992). The far-field harmonic field $E_q(r', z')$ is obtained from the harmonic field at the exit of the medium $E_q(r, z)$ through a Hankel transformation (Siegman 1986):

$$E_q(r', z') = -\mathrm{i}k_q \int \frac{E_q(r, z)}{z' - z} J_0\left(\frac{k_q r r'}{z' - z}\right) \exp\left[\frac{\mathrm{i}k_q(r^2 + r'^2)}{2(z' - z)}\right] r \, \mathrm{d}r$$

where k_q is the harmonic wave vector and J_0 the zero-order Bessel function.

The parameters are chosen to mimic the experimental conditions. The gas density distribution is modelled by a truncated Lorentzian function with a full width at half maximum L of 0.8 mm and a total width of 1.6 mm. The laser beam is assumed to be Gaussian in time and space, with a confocal parameter b of 5 mm.

6.2. Simulation of the z-dependence

Figure 13 presents the spatial profile for the 39th harmonic generated in neon at 3×10^{14} W cm^{-2} as a function of the z position of the generating medium relative to the laser focus. The simulated profiles reproduce remarkably well the distortion as well as the divergence of the experimental profiles of figure 3, but for a smaller step in z: 0.75 mm instead of 1 mm. The total evolution is thus spread on 3.75 mm instead of the experimental 5 mm.

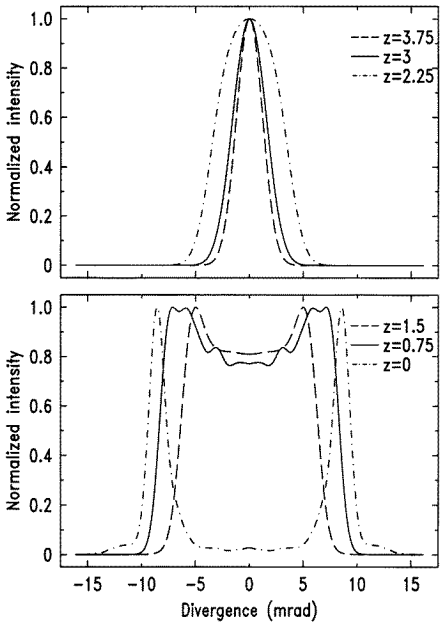

Figure 13. Simulated spatial profiles of the 39th harmonic generated in neon at a peak intensity of 3×10^{14} W cm^{-2} for different locations z of the medium relative to the laser focus, indicated in mm in the figure.

However, the experimental precision on the determination of the characteristic lengths of the interaction, namely L for the nonlinear medium and b for the laser beam, is not very good. Therefore, we have examined the incidence on the spatial profiles of the variations of both L and b. We found, as shown in the appendix, that under certain conditions (negligible dispersion and absorption), the harmonic profile is independent of the ratio b/L, if appropriately scaled. More precisely, the multiplication of both characteristic lengths L and b by the same factor μ leads to the same angular profile provided (r, z) are changed to $(r' = r \times \sqrt{\mu}, z' = z \times \mu)$. Thus the spatial profile of a harmonic emitted from a jet at position μz will present the same shape as that from a jet at position z (with the former characteristics) but with a divergence bigger by a factor of $\sqrt{\mu}$. Note that the conversion efficiency is increased by a factor of μ^3 (for the same peak density). By multiplying L and b by $\frac{4}{3}$, which gives respectively 1.1 mm and 6.7 mm, the evolution is now the same as that in figure 13 but with a 1 mm step, while the divergence of the profiles is slightly increased by a factor of 1.15. Our experimental precision on both L and b does not allow us to decide between these values and the former ones.

Moreover, there are additional sources of discrepancy. Indeed, whilst the Lorentzian distribution seems to be a good approximation of the gas density profile (Altucci *et al* 1996), the laser was far from being a lowest-order Gaussian beam. As mentioned above, the laser beam was about three times diffraction limited, which means that the angular spread was larger than the diffraction associated with the beam size at focus. Moreover, the laser beam presented some astigmatism. All of this can clearly influence the harmonic far-field distributions. Generally speaking, any inhomogeneity of the gas density or of the laser spot intensity distribution is expected to distort the harmonic profiles owing to the nonlinearities involved. These harmonic profiles are thus a very sensitive test of the interaction, and the agreement obtained here with a rather simple modelling is more than satisfactory.

This dramatic dependence on the focusing geometry can be explained in terms of the behaviour of the phase of the harmonic dipole moment in the tunnelling regime

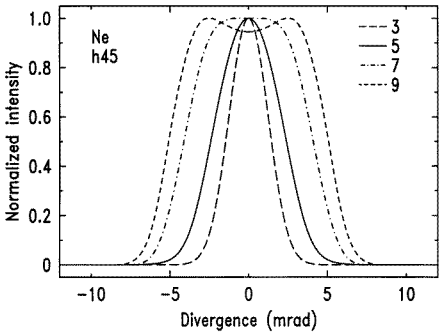

Figure 14. Simulated spatial profiles of the 45th harmonic generated in neon at $z = 3$ mm for different laser intensities indicated in units of 10^{14} W cm^{-2} in the figure.

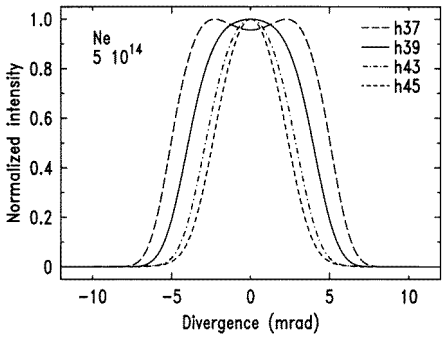

Figure 15. Simulated spatial profiles of harmonics located between the 37th and the 45th, generated in neon at $z = 3$ mm and at an intensity of 5×10^{14} W cm^{-2}.

(Salières *et al* 1995, Lewenstein *et al* 1995). In the cut-off region, it decreases slowly but linearly with intensity, whereas in the plateau, the decrease is twice as fast with superimposed oscillations. The longitudinal intensity distribution around the laser focus induces a corresponding distribution of the harmonic emission phases which influences the phase matching between the nonlinear polarization and the propagating harmonic field. Before the focus, this emission phase variation adds to that induced by the phase shift of the fundamental field, resulting on axis in a quick decrease of the total phase. Efficient phase matching is thus prevented on axis, but can be realized off axis, leading to annular profiles. After the focus, the variations of both phases have opposite signs and compensate when the intensity on axis corresponds to the cut-off region (where the dipole phase varies more slowly). Consequently, by placing the medium sufficiently after the focus, a good phase matching on axis is achieved resulting in very regular Gaussian profiles. In between these two positions, the continuous distortion of the harmonic profile reflects the variation of phase matching in the nonlinear medium.

6.3. Simulation of the intensity dependence

Figure 14 shows the spatial profile for the 45th harmonic generated in neon at $z = 3$ mm as a function of the laser intensity (at focus) indicated in units of 10^{14} W cm^{-2} in the caption. The divergence increases first quickly, from 5 mrad at 3×10^{14} W cm^{-2} to 11 mrad at 7×10^{14} W cm^{-2}, while the profile evolves from Gaussian to near flat-top. Then the increase of the divergence is less rapid and a small dip appears at the centre of the profile. We thus reproduce the divergence and shape of the experimental distributions represented in figure 5, except for the latter distortion, too weak perhaps to be clearly visible in the experiment.

As mentioned above, the regularity of the profiles for this focus position is related to the slow intensity dependence of the dipole phase in the cut-off region. However, the amplitude of the dipole in this region is very small. Indeed, it increases very steeply with intensity until the plateau is reached, where it saturates, exhibiting many interferences. Therefore, it is the transition region between cut-off and plateau, where the amplitude is already high and the phase still slow, that contributes mainly to the harmonic production. Increasing the intensity at focus moves the position of this transition region in the medium. The harmonic profiles are broadened when this region reaches the high-density zone at the centre of the gas jet.

6.4. Simulation of the order dependence

Figure 15 presents the harmonic profiles obtained at 5×10^{14} W cm^{-2} in neon for $z = 3$ mm. The divergence of the profiles decreases with increasing order. The agreement with the behaviour exhibited by the experimental profiles (see figures 9–10) is reasonably good. Note that the theoretical results are closer to the experimental ones at 2.7×10^{14} W cm^{-2} than to those obtained at the same nominal intensity. This difference can be attributed both to the limitations in the determination of the experimental parameters as well as to the simplifications of the model (assuming for example a diffraction-limited laser beam).

The observed variation of the divergence with the nonlinear order is clearly connected to the different intensities of the plateau–cut-off transition for the different harmonics. These transition intensities increase with order. Thus, when the intensity in the medium corresponds to the transition region of the 39th harmonic, for instance, resulting in a large divergence, the 45th harmonic is far in the cut-off, with a narrow distribution.

Generally speaking, the similarity of all these profiles is due to the universal behaviour of the dipole moment in the tunnelling regime, independently of the (sufficiently high) order or the nature of the gas. The main difference between dipoles associated with different orders (and gases) is the transition intensity between the cut-off and plateau regions. We thus obtain similar trends, but shifted in order or in intensity depending on the studied parameter.

7. Conclusion

Using a short-pulse laser, we have shown experimentally that it is possible to generate harmonic beams with very regular, structureless spatial profiles. The distributions vary from Gaussian for harmonics in the cut-off region to triangular or super-Gaussian in the plateau respectively in argon and neon. The divergence of the profiles is mainly determined by the region of the spectrum—cut-off or plateau—the harmonic belongs to, and not *directly* by parameters such as nonlinear order, intensity or nature of the gas.

These regular profiles are obtained for a focus position sufficiently *before* the nonlinear medium. When the focus is drawn closer to the jet, the distributions get broadened and increasingly distorted. When finally the focus is in—or after—the jet, the profiles are annular with a big divergence. There is thus a dramatic dependence of the angular distributions on the focusing geometry.

We have simulated these harmonic spatial profiles using dipole moments calculated in the tunnelling regime, and a propagation code. The simulated profiles reproduce remarkably well all the experimental trends, allowing us to interpret them. The regular profiles are obtained when the intensity *in the medium* corresponds to the plateau–cut-off transition in the intensity dependence of the considered harmonic. They result from a good phase matching on axis, induced by the slow variation of the atomic phase, and from the regular variation of the dipole amplitude in this region. In the tunnelling regime, the harmonic dipoles generated in different gases have a similar behaviour, and their main difference is the transition intensity between the cut-off and plateau regions. This is the reason for the similarity of the profiles and their main dependence on the region of the spectrum the considered harmonic belongs to. For a focusing into—or after—the jet, the quick variation of the polarization phase on axis prevents an efficient phase matching, that can still be realized off axis. The resulting profiles are annular with a large divergence.

Thus, these characterization experiments have resulted in a better understanding of the

physics of high-order harmonic generation, and especially of the importance of the dipole phase in the tunnelling regime.

Acknowledgments

We are grateful to K Budil and A Sanchez for their help during the early stages of this experiment. The experimental work was performed at the Lawrence Livermore National Laboratory under the auspices of the US Department of Energy under contract W-7405-Eng-48. We also acknowledge the support from the Direction des Recherches, Etudes et Techniques under contract 92-439.

Appendix

In the following, we establish scaling laws corresponding to variations of the characteristic lengths of the interaction: density distribution length and confocal parameter of the laser beam. All density effects are neglected, such as absorption, atomic and electronic dispersion, defocusing of the laser, etc. We thus consider low atomic densities and small ionization rates.

In these conditions, we can use an integral formalism of the propagation equation of the harmonic beam (L'Huillier *et al* 1991), which gives the harmonic far-field distribution as

$$E_q(r', z') = \left(\frac{q\omega}{c}\right)^2 \int \frac{P_q(r, z)}{z' - z} \exp\left[\frac{\mathrm{i}k_q(r^2 + r'^2)}{2(z' - z)}\right] J_0\left(\frac{k_q r r'}{z' - z}\right) 2\pi r \,\mathrm{d}r \,\mathrm{d}z$$

where J_0 is the zero-order Bessel function and $P_q(r, z)$, the nonlinear polarization. The latter is determined by the spatial distributions of the gas density and of the laser beam. The gas density $\mathfrak{n}$ is generally supposed to be constant in the transverse direction, given the small laser spot size, whereas its longitudinal profile presents a characteristic length L. As for the lowest-order Gaussian laser field E_1, its longitudinal variation (in phase and amplitude) is governed by the confocal parameter b, and the radial distribution, by $\sqrt{b}$. We can thus write

$$P_q\left[\mathfrak{n}\left(\frac{z - z_0}{L}\right), E_1\left(\frac{r}{\sqrt{b}}, \frac{z}{b}\right)\right]$$

z_0 being the position of the jet centre relative to the laser focus (placed in $z = 0$).

Let us introduce the reduced quantities $R = r/\sqrt{b}$, $R' = r'/\sqrt{b}$, $Z = z/b$, $Z' = z'/b$, $Z_0 = z_0/b$. (The truly reduced quantities are obviously $R = r/\sqrt{\lambda b}$ and $R' = r'/\sqrt{\lambda b}$, but we drop $\sqrt{\lambda}$ for clarity.) The harmonic field is then written

$$E_q\left(\sqrt{b}R', bZ'\right) = b\left(\frac{q\omega}{c}\right)^2 \int \frac{1}{Z' - Z} P_q\left[\mathfrak{n}\left(\frac{b}{L}(Z - Z_0)\right), E_1(R, Z)\right] \times \exp\left[\frac{\mathrm{i}k_q(R^2 + R'^2)}{2(Z' - Z)}\right] J_0\left(\frac{k_q R R'}{Z' - Z}\right) 2\pi R \,\mathrm{d}R \,\mathrm{d}Z$$

or

$$E_q\left(\sqrt{b}R', bZ'\right) = b \times G_q\left(R', Z', Z_0, \frac{b}{L}\right),$$

where G_q depends only on reduced quantities.

If we consider the case where both characteristic lengths b and L are multiplied by a factor μ, while keeping the same peak density and peak intensity, the harmonic field for a jet centre position in $\mu \times z_0$ is written

$$E_q\left(\sqrt{\mu}\sqrt{b}R', \mu b Z'\right) = \mu \times E_q\left(\sqrt{b}R', bZ'\right).$$

The angular distribution of the harmonic field is thus the same, if appropriately scaled. The increase in the field amplitude by a factor μ results from the increase of the coherence length. Thus the symmetry of the interaction is preserved by inducing the change of scale: $(r, z) \Rightarrow (r \times \sqrt{\mu}, z \times \mu)$. This property is used in section 6.2 for the comparison of the simulated and experimental spatial profiles.

The number of generated harmonic protons is written

$$N_q = \frac{\epsilon_0 \pi c}{\hbar q \omega} \int |E_q(r', z', t)|^2 r' \,\mathrm{d}r' \,\mathrm{d}t = b^3 \frac{\epsilon_0 \pi c}{\hbar q \omega} \int \left| G_q\left(R', Z', Z_0, \frac{b}{L}, t\right)\right|^2 R' \,\mathrm{d}R' \,\mathrm{d}t$$

or $N_q = b^3 \times \mathbb{N}_q$, where $\mathbb{N}_q$ depends only on reduced quantities (except for the time). In the conditions studied above, the number of generated protons is thus multiplied by a factor of μ^3.

If we now consider a variation of the confocal parameter b while keeping the density distribution unchanged, the 'b^3 law' is, strictly speaking, no longer valid. However it still applies in some conditions like a tight focusing at the centre of the jet. Indeed, if the harmonic dipole moment varies sufficiently quickly with intensity, its value will be high on a small interval around the focus, thus at the central part of the density distribution. The limiting factor is then the dipole moment and not the density, even though the latter has not been increased like b. However if we keep increasing b, the variation of the dipole moment in the medium becomes more and more slow, and the—too narrow—density distribution begins to limit the harmonic generation process. The increase in number of generated photons follows then a 'b law', corresponding to the increase of the laser section. In this particular case, we thus reach the same conclusions as those obtained with intuitive arguments by Balcou *et al* (1992).

References

Altucci C, Starczewski T, Wahlström C-G, Merel E, Carré B and L'Huillier A 1996 *J. Opt. Soc. Am.* B **13** 148

Balcou Ph, Cornaggia C, Gomes A S L, Lompré L A and L'Huillier A 1992 *J. Phys. B: At. Mol. Opt. Phys.* **25** 4467

Corkum P B 1993 *Phys. Rev. Lett.* **73** 1995

Ditmire T, Nguyen H and Perry M D 1994 *J. Opt. Soc. Am.* B **11** 580

Kulander K C, Schafer K J and Krause J L 1993 *Super-Intense Laser-Atom Physics (NATO ASI Series B)* vol 316, ed B Piraux, A L'Huillier and K Rzazewski (New York: Plenum) p 95

Lewenstein M, Balcou Ph, Ivanov M Yu, L'Huillier A and Corkum P B 1994 *Phys. Rev.* A **49** 2117

Lewenstein M, Salières P and L'Huillier A 1995 *Phys. Rev.* A **52** 4747

L'Huillier A, Schafer K J and Kulander K C 1991 *J. Phys. B: At. Mol. Opt. Phys.* **24** 3315

L'Huillier A, Balcou Ph, Candel S, Schafer K J and Kulander K C 1992 *Phys. Rev.* A **46** 2778

L'Huillier A and Balcou Ph 1993 *Laser Phys.* **3** 654

Macklin J J, Kmetec J D and Gordon III C L 1993 *Phys. Rev. Lett.* **70** 766

Muffet J E, Wahlström C-G and Hutchinson M H R 1994 *J. Phys. B: At. Mol. Opt. Phys.* **27** 5693

Peatross J and Meyerhofer D D 1995 *Phys. Rev.* A **51** R906

Preston S G *et al* 1996 *Phys. Rev.* A **53** R31

Salières P, Ditmire T, Budil K S, Perry M D and L'Huillier A 1994 *J. Phys. B: At. Mol. Opt. Phys.* **27** L217

Salières P, L'Huillier A and Lewenstein M 1995 *Phys. Rev. Lett.* **75** 3776

Siegman A E 1986 *Lasers* (Mill Valley, CA: University Science)

Tisch J W G, Smith R A, Muffet J E, Ciarocca M, Marangos J P and Hutchinson M H R 1994 *Phys. Rev.* A **49** R28

Wahlström C-G, Borgström S, Larsson J and Pettersson S-G 1995 *Phys. Rev.* A **51** 585

Wahlström C-G, Larsson J, Persson A, Starczewski T, Svanberg S, Salières P, Balcou Ph and L'Huillier A 1993 *Phys. Rev.* A **48** 4709